Journal of Computational Physics **173,** 455–480 (2001)
doi:10.1006/jcph.2001.6887, available online at http://www.idealibrary.com on IDEAL®

A Stable, Perfectly Matched Layer for Linearized Euler Equations in Unsplit Physical Variables

Fang Q. Hu

Department of Mathematics and Statistics, Old Dominion University, Norfolk, Virginia 23529
E-mail: fhu@odu.edu

Received April 4, 2001; revised July 20, 2001

The instability of an earlier perfectly matched layer (PML) formulation for the linearized Euler equations is investigated. It is found that, in the presence of a mean flow, there exist acoustic waves that have a positive group velocity but a negative phase velocity in the direction of the mean flow and these waves become actually amplified in the previous formulation, thus giving rise to the instability. A new stable PML formulation that is perfectly matched to the Euler equations and does not entail exponentially growing solution is presented. Furthermore, the new formulation is given in unsplit physical variables which should facilitate its implementation in many practical schemes. In addition, the well-posedness of the new formulation is also considered. It is shown that the proposed equations are well-posed for horizontal y-layers but weakly well-posed for vertical x-layers and corner layers. However, it is further shown that they can be easily modified to be symmetrizable, thus strongly well-posed, by an addition of arbitrarily small terms. Numerical examples that verify the stability and effectiveness of the proposed PML equations, such as an absorbing boundary condition, are given.

Key Words: nonreflecting boundary conditions; Euler equations; computational acoustics.

1. INTRODUCTION

In numerical simulations with an open domain, such as those that occur in many practical problems in computational acoustics and computational fluid dynamics, it is crucial to have accurate nonreflecting boundary conditions for achieving time-accurate solutions. Quite often, nonreflecting boundaries are the sources of the most significant numerical errors in a computation. This is especially true after the substantial progress in recent years in the discretization methods, such as the utilization of high-order schemes and unstructured meshes as well as the orders-of-magnitude increase in high-performance computing power.

0021-9991/01 $35.00

A variety of nonreflecting boundary conditions have been developed in the literature to cope with the open-domain problem. The most widely used nonreflecting boundary conditions for the Euler equations are the characteristics-based inflow and outflow boundary conditions [1–4]. These methods are formed by a generalization of one-dimensional Euler equations to the multidimensional cases. The use of characteristics variables is usually straightforward and robust, especially for schemes with upwinding features. The drawback of the characteristics-based boundary conditions is that the accuracy can be limited. They usually work best when the wave angle is normal to the boundary, and their performances can deteriorate when the wave angles deviate from that of a normal incident.

Another type of widely used nonreflecting boundary condition is based on the far-field asymptotic solutions [5–8]. The governing equations at the boundary are replaced by suitable forms of modified partial differential equations based on the asymptotic form of the solution at the far field. This class of methods, when applicable, can be quite accurate. However, because the asymptotic forms are not always available, this type of boundary conditions may not be applicable in many situations. In addition, to implement the asymptotic solution-based boundary conditions the computational boundary is necessarily placed at far field to achieve the accuracy. This can result in an increase in computational cost.

A third type of nonreflecting boundary condition is the buffer zone technique, which is actually a group of methods based on various buffer zone techniques. For instance, the computational domain may be extended to create an extra zone where the numerical solution is damped by an application of low-pass filters, grid stretching, numerical damping, or a combination of these techniques [9, 10]; or the mean flow is accelerated to a supersonic velocity toward the end of the added buffer domain, thus eliminating the need for a nonreflecting boundary condition [11, 12]. The accuracy of these methods depends on the gradualness in which the various parameters are varied inside the buffer zone. Moreover, the added buffer zone usually is required to be of substantial length for the method to be effective. The increase in computational cost can be significant.

A recently emerged method of constructing a nonreflecting boundary condition is based on the perfectly matched layer (PML) technique [13]. In this approach, as in the buffer zone method, extra layers of grids are added to the nonreflecting boundaries in which the outgoing waves are damped or "absorbed." A major difference between the PML technique and the other buffer zone techniques mentioned earlier is that the equations to be used in the added region are constructed in such a way that, theoretically, the outgoing waves will not cause any reflection when entering a PML domain for any frequency and angle of incidence. Because of this, a PML domain usually is very effective as an absorbing boundary condition and requires only a small number of grid points to achieve satisfactory results [14, 15].

The PML technique was first introduced by Berenger [13] for absorbing electromagnetic waves of the Maxwell equations. For the Euler equations there currently are two main PML formulations. The first formulation was given by the author in [14]. Like Berenger's original formulation for the Maxwell equations, it used split variables in the PML domain; i.e., the velocity, pressure, and density were split into two independent parts according to the spatial derivative terms in the Euler equations in two space dimensions. The second formulation was given by Abarbanel *et al.* [16]. This formulation did not split the physical variables but instead augmented the Euler equations with additional terms, albeit complicated, so that all waves decayed exponentially inside the PML domain. There

also are other formulations, notably those by Turkel and Yefet [17] that are aimed at absorbing only the convective acoustic waves when the vorticity and entropy waves are not present.

Unfortunately, both formulations given in [14] and [16] entail exponentially growing solutions that, if not suppressed or eliminated by numerical dissipation or other means, can cause numerical instability in the PML domain and ruin the numerical solution. In [14], the instabilities were suppressed by a use of numerical filtering. In [16], artificial damping terms were added to the PML equations. The instability waves of the PML equations formulated in [14] have been studied at length by Tam *et al.* [18]. They analyzed the dispersion relations of the linear waves and found that the PML equations of [14] have unstable solutions whenever the mean flow has a component normal to the PML domain interface. They suggested a use of artificial selective damping for the suppression of instability waves, since the unstable modes were associated with high wavenumbers.

In addition to the instability issue, there also is a well-posedness issue for the formulation given in [14]. The original PML equations constructed by Berenger [13] for the Maxwell equations were shown to be only weakly well-posed by Abarbanel and Gottlieb [19]. Later, it was shown by Hesthaven [20] that the formulation given in [14] for the Euler equations was also only weakly well-posed. It was demonstrated that the PML equations proposed in [13] and [14] could become ill-posed by certain low-order perturbations. These authors attributed the weakly well-posedness, in part, to the fact that PML equations in [13] and [14] were constructed by splitting the physical variables. This prompted them to construct PML equations without splitting the physical variables in [16]. However, as mentioned earlier, although the equations given in [16] were shown to be well-posed, they also admitted exponentially growing solutions. A close inspection of the analysis presented in [16] indicates that the unstable modes are associated with low wave numbers. In this case, exponentially growing solutions can be found for $k = 0$, where k is the spatial wave number.

In this paper, we address both the stability and the well-posedness issues related to the formulation given in [14]. We investigate the cause of the instability and develop a new stable PML formulation. Since the publication of Berenger's paper [13], many further studies on the PML technique appeared in the literature. Most of the works, however, were done in the context of solving the Maxwell equations. Several of these studies indicated that the PML technique can be viewed, at least mathematically, as a complex change of variables in space (e.g., [17, 21–24]). This view is extended to the study of the Euler equations and is instrumental in constructing the unsplit PML equations presented here.

The content of the paper is organized as follows: After a brief review of the linear waves and their dispersion relations supported by the Euler equations in Section 2, we show in Section 3 that the splitting of physical variables is not essential when the PML technique is viewed as a complex change of variables and an unsplit reformulation of [14] is given. In Section 4, we study the cause of the instability found in the formulation given in [14] (as well as its reformulation) and offer an explanation on the origin of the instability. In Section 5, utilizing a coordinate transformation, a stable PML formulation for the Euler equations is developed. The well-posedness issue of the new formulation is studied and discussed in Section 6. Numerical examples that verify the stability and effectiveness of the new formulation are presented in Section 7. Section 8 has the concluding remarks.

2. PLANE WAVES OF THE EULER EQUATIONS

We consider the linearized Euler equations with a uniform mean flow in a vector form

$$\frac{\partial \mathbf{u}}{\partial t} + \mathbf{A}\frac{\partial \mathbf{u}}{\partial x} + \mathbf{B}\frac{\partial \mathbf{u}}{\partial y} = 0, \tag{1}$$

where

$$\mathbf{u} = \begin{pmatrix} \rho \\ u \\ v \\ p \end{pmatrix}, \quad \mathbf{A} = \begin{pmatrix} M & 1 & 0 & 0 \\ 0 & M & 0 & 1 \\ 0 & 0 & M & 0 \\ 0 & 1 & 0 & M \end{pmatrix}, \quad \mathbf{B} = \begin{pmatrix} 0 & 0 & 1 & 0 \\ 0 & 0 & 0 & 0 \\ 0 & 0 & 0 & 1 \\ 0 & 0 & 1 & 0 \end{pmatrix}. \tag{2}$$

Here, ρ is the density, (u, v) is the velocity vector, p is the pressure, and M is the Mach number (i.e., the mean flow nondimensionalized by the speed of sound). We also assume that the mean flow is subsonic; i.e., $M < 1$.

It is well known that, when we look for plane waves of the form $\mathbf{u}_0 e^{ik_x x + ik_y y - i\omega t}$, the Euler equations support three types of waves: acoustic, vorticity, and entropy. In particular, the dispersion relations for these waves are

$$(\omega - Mk_x)^2 - k_x^2 - k_y^2 = 0 \tag{3}$$

for the acoustic waves and

$$\omega - Mk_x = 0 \tag{4}$$

for the vorticity and entropy waves.

For convenience of discussion, we use the dispersion relations to express the wave numbers k_x and k_y in terms of the frequency ω and a wave angle ϕ; i.e., we have

$$k_x = \frac{\omega \cos\phi}{1 + M\cos\phi}, \quad k_y = \frac{\omega \sin\phi}{1 + M\cos\phi} \tag{5}$$

for the acoustic waves and

$$k_x = \frac{\omega}{M}, \quad k_y = \frac{\omega \tan\phi}{M} \tag{6}$$

for the vorticity and entropy waves [25]. Then the plane wave solutions of the Euler equations are found to be

$$\begin{pmatrix} \rho \\ u \\ v \\ p \end{pmatrix} = A \begin{pmatrix} 1 \\ \cos\phi \\ \sin\phi \\ 1 \end{pmatrix} \exp\left(\frac{i\omega\cos\phi}{1 + M\cos\phi} x + \frac{i\omega\sin\phi}{1 + M\cos\phi} y - i\omega t \right) \quad \text{(acoustic)}, \tag{7}$$

$$\begin{pmatrix} \rho \\ u \\ v \\ p \end{pmatrix} = B \begin{pmatrix} 0 \\ -\sin\psi \\ \cos\psi \\ 0 \end{pmatrix} \exp\left(\frac{i\omega}{M} x + \frac{i\omega\tan\psi}{M} y - i\omega t \right) \quad \text{(vorticity)}, \tag{8}$$

$$\begin{pmatrix} \rho \\ u \\ v \\ p \end{pmatrix} = C \begin{pmatrix} 1 \\ 0 \\ 0 \\ 0 \end{pmatrix} \exp\left(\frac{i\omega}{M} x + \frac{i\omega \tan\chi}{M} y - i\omega t \right) \qquad \text{(entropy)}, \tag{9}$$

where ϕ, ψ, and χ are the angles of the wave-front normal vectors of the acoustic (A), vorticity (B), and entropy (C) waves, respectively. We note that the wave angles are not assumed to be the same since the three types of waves are kept independent of each other.

3. AN UNSPLIT FORMULATION

In the PML methodology, absorbing layers are added to the Euler domain so that all three wave types mentioned in Section 2 are absorbed without reflection. The added PML domains, shown in Fig. 1 (see also Fig. 6), are referred to as horizontal y-layers, vertical x-layers, or corner layers. A straightforward extension of the PML technique originally proposed by Berenger [13] for the Maxwell equations suggests a splitting of the Euler equations according to the spatial derivative terms [14]. This results in the split version of the PML equations for (1),

$$\frac{\partial \mathbf{u}_1}{\partial t} + \sigma_x \mathbf{u}_1 + \mathbf{A}\frac{\partial \mathbf{u}}{\partial x} = 0, \tag{10}$$

$$\frac{\partial \mathbf{u}_2}{\partial t} + \sigma_y \mathbf{u}_2 + \mathbf{B}\frac{\partial \mathbf{u}}{\partial y} = 0, \tag{11}$$

where $\mathbf{u} = \mathbf{u}_1 + \mathbf{u}_2$. σ_x and σ_y are positive absorption coefficients. The conditions on the absorption coefficients are that σ_x be independent of y and σ_y be independent of x with both being assumed zero in the interior Euler domain. As shown in [14] (or [15] for a more general case), (10) and (11) are perfectly matched to the Euler equations in the rectangular Cartesian coordinates. That is, theoretically an acoustic, vorticity, or entropy wave can enter a PML domain without reflection.

However, as mentioned in the Section 1, Eqs. (10) and (11) admit instability waves which, if not suppressed by numerical dissipation or other means, could ruin the numerical solution. In addition, (10) and (11) are only weakly well-posed and can become ill-posed under certain low-order perturbations on the split variables [20]. We show next, however, that the splitting of the physical variables is not essential and an alternative formulation that is equivalent to (10) and (11) but uses unsplit physical variables may be found by introducing an auxiliary variable.

We begin by examining the PML technique as a complex change of variables for x and y. Let us consider the split version (10) and (11) in the frequency domain. By replacing $\frac{\partial}{\partial t}$ with $-i\omega$, we get

$$-i\omega \tilde{\mathbf{u}}_1 + \sigma_x \tilde{\mathbf{u}}_1 + \mathbf{A}\frac{\partial \tilde{\mathbf{u}}}{\partial x} = 0, \tag{12}$$

$$-i\omega \tilde{\mathbf{u}}_2 + \sigma_y \tilde{\mathbf{u}}_2 + \mathbf{B}\frac{\partial \tilde{\mathbf{u}}}{\partial y} = 0, \tag{13}$$

where a tilde indicates the solution in the frequency domain. Dividing Eqs. (12) and (13) by $1 + i\sigma_x/\omega$ and $1 + i\sigma_y/\omega$, respectively, and subsequently adding the two equations, we

get an equation in the unsplit physical variables:

$$-i\omega\tilde{\mathbf{u}} + \frac{1}{1+\frac{i\sigma_x}{\omega}}\mathbf{A}\frac{\partial\tilde{\mathbf{u}}}{\partial x} + \frac{1}{1+\frac{i\sigma_y}{\omega}}\mathbf{B}\frac{\partial\tilde{\mathbf{u}}}{\partial y} = 0. \tag{14}$$

Thus, if we introduce a complex change of variables for x and y as

$$x' = \left(1+\frac{i\sigma_x}{\omega}\right)x, \quad y' = \left(1+\frac{i\sigma_y}{\omega}\right)y, \tag{15}$$

Eq. (14) becomes simply

$$-i\omega\tilde{\mathbf{u}} + \mathbf{A}\frac{\partial\tilde{\mathbf{u}}}{\partial x'} + \mathbf{B}\frac{\partial\tilde{\mathbf{u}}}{\partial y'} = 0. \tag{16}$$

It is easy to see that this is exactly the same as the Euler equations when (1) is written in the frequency domain and x and y are replaced by x' and y', respectively. Therefore, the plane wave solutions of (16) should be the same as those in (7)–(9), with x and y being replaced by x' and y'. That is, the plane waves of (16), and thus the PML equations (10) and (11), will be

$$\begin{pmatrix}\rho\\ u\\ v\\ p\end{pmatrix} = A\begin{pmatrix}1\\ \cos\phi\\ \sin\phi\\ 1\end{pmatrix}\exp\left(\frac{i\omega\cos\phi}{1+M\cos\phi}x - \frac{\sigma_x\cos\phi}{1+M\cos\phi}x + \frac{i\omega\sin\phi}{1+M\cos\phi}y\right.$$
$$\left. - \frac{\sigma_y\sin\phi}{1+M\cos\phi}y - i\omega t\right) \qquad \text{(acoustic)}, \tag{17}$$

$$\begin{pmatrix}\rho\\ u\\ v\\ p\end{pmatrix} = B\begin{pmatrix}0\\ -\sin\psi\\ \cos\psi\\ 0\end{pmatrix}\exp\left(\frac{i\omega}{M}x - \frac{\sigma_x}{M}x + \frac{i\omega\tan\psi}{M}y\right.$$
$$\left. - \frac{\sigma_y\tan\psi}{M}y - i\omega t\right) \qquad \text{(vorticity)}, \tag{18}$$

$$\begin{pmatrix}\rho\\ u\\ v\\ p\end{pmatrix} = C\begin{pmatrix}1\\ 0\\ 0\\ 0\end{pmatrix}\exp\left(\frac{i\omega}{M}x - \frac{\sigma_x}{M}x + \frac{i\omega\tan\chi}{M}y - \frac{\sigma_y\tan\chi}{M}y - i\omega t\right) \qquad \text{(entropy)}. \tag{19}$$

Here σ_x and σ_y play the role of the exponential decaying rate while both the wave angles and the wave vectors (or eigenvectors of (14)) are unchanged. These solutions are perfectly matched to (7)–(9). In fact, (17)–(19) are exactly the same solutions as those given in [14] when expressed in the unsplit variables.

To implement the PML in the unsplit physical variables, we multiply (14) by $(1+i\sigma_x/\omega)(1+i\sigma_y/\omega)$ and readily get

$$-i\omega\tilde{\mathbf{u}} + (\sigma_x+\sigma_y)\tilde{\mathbf{u}} + \frac{i\sigma_x\sigma_y}{\omega}\tilde{\mathbf{u}} + \mathbf{A}\frac{\partial\tilde{\mathbf{u}}}{\partial x} + \frac{i\sigma_y}{\omega}\mathbf{A}\frac{\partial\tilde{\mathbf{u}}}{\partial x} + \mathbf{B}\frac{\partial\tilde{\mathbf{u}}}{\partial y} + \frac{i\sigma_x}{\omega}\mathbf{B}\frac{\partial\tilde{\mathbf{u}}}{\partial y} = 0. \tag{20}$$

This can be written back in the time domain by introducing an auxiliary variable $\mathbf{q}$ below. Thus, a reformulation of (10) and (11) using the unsplit physical variables is constructed as

$$\frac{\partial \mathbf{u}}{\partial t} + \mathbf{A}\frac{\partial \mathbf{u}}{\partial x} + \mathbf{B}\frac{\partial \mathbf{u}}{\partial y} + \sigma_y \mathbf{A}\frac{\partial \mathbf{q}}{\partial x} + \sigma_x \mathbf{B}\frac{\partial \mathbf{q}}{\partial y} + (\sigma_x + \sigma_y)\mathbf{u} + \sigma_x \sigma_y \mathbf{q} = 0, \tag{21}$$

$$\frac{\partial \mathbf{q}}{\partial t} = \mathbf{u}. \tag{22}$$

Obviously, (21) and (22) admit the same plane wave solutions as that of the split version (10) and (11) because of their equivalence in the frequency domain. It follows that (21) and (22) are, too, perfectly matched to the Euler equations.

It is important to note that the auxiliary variable $\mathbf{q}$ is needed only inside the PML domains because the spatial derivative $\frac{\partial \mathbf{q}}{\partial x}$ is required only when $\sigma_y \neq 0$, which happens only inside a horizontal y-layer or corner layer and $\frac{\partial \mathbf{q}}{\partial y}$ is required only when $\sigma_x \neq 0$ inside a vertical x-layer or corner layer. This situation is illustrated in Fig. 1. As a result, we do not need to know $\mathbf{q}$ in the Euler domain. Therefore, $\mathbf{q}$ is neither computed nor stored inside the Euler domain.

However, although Eqs. (21) and (22) are now cast in the unsplit physical variables, the instability issue remains, since both the split and unsplit versions have the same dispersion relations by which the stability of the partial differential equations is determined. In the next section, we offer an explanation of the cause of this instability and, in Section 5, we develop a stable PML formulation. As we will see, the stable PML formulation adds only one more term to Eq. (21).

We also point out that the change of variables suggested in (15) can be extended to include the cases in which the absorption coefficients σ_x and σ_y are functions of x and y, respectively [17, 21]. For simplicity, however, they are treated as constant in the present analysis.

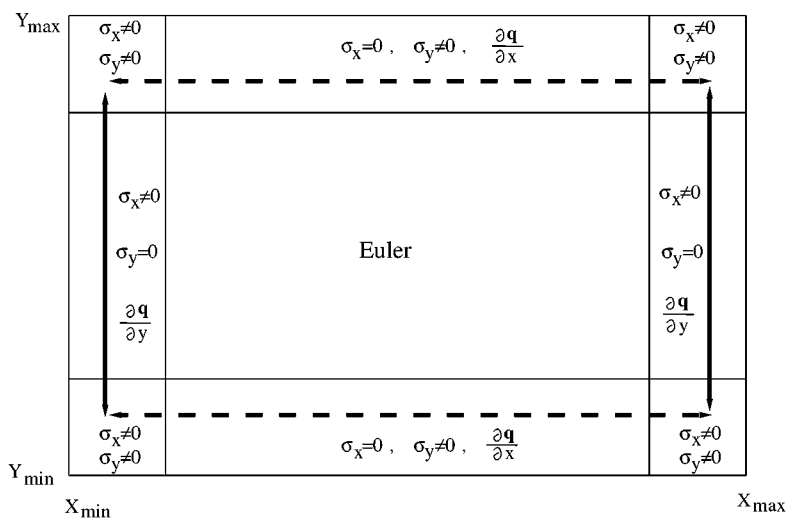

FIG. 1. Illustration of a computational domain combining the Euler and PML domains. Solid arrowed lines indicate the domains where $\partial \mathbf{q}/\partial y$ is needed and dashed arrowed lines indicate the domains where $\partial \mathbf{q}/\partial x$ is needed.

4. THE INSTABILITY AND ITS CAUSE

Under the complex change of variables (15), the dispersion relations for (21) and (22) can be found simply by replacing k_x and k_y in (3) and (4) with the expressions

$$k_x \to \frac{k_x}{1+\frac{i\sigma_x}{\omega}}, \quad k_y \to \frac{k_y}{1+\frac{i\sigma_y}{\omega}}. \tag{23}$$

This results in

$$\left(\omega - M\frac{k_x}{1+\frac{i\sigma_x}{\omega}}\right)^2 - \left(\frac{k_x}{1+\frac{i\sigma_x}{\omega}}\right)^2 - \left(\frac{k_y}{1+\frac{i\sigma_y}{\omega}}\right)^2 = 0 \tag{24}$$

for the acoustic waves and

$$\omega - M\frac{k_x}{1+\frac{i\sigma_x}{\omega}} = 0 \tag{25}$$

for the vorticity and entropy waves supported by (21) and (22). They are, of course, the same as those of (10) and (11) given in [14] or [18].

As pointed out in [18], for certain real values of k_x and k_y, (24) has complex ω with a positive imaginary part, thus exponentially growing solutions. In Fig. 2, we plot the contours of the maximum growth rate ω_i, the imaginary part of ω, as a function of the mean-flow Mach number M and absorption coefficient σ_x (with $\sigma_y = 0$) for a chosen range of wavenumbers $|k_x| \le 5$ and $|k_y| \le 5$. As we can see, the growth rate increases with M and σ_x. Thus, in practical computations, it would be difficult to suppress the instability occurring in flows with a high Mach number.

To understand the cause of this instability, we reexamine the exponent in the PML acoustic wave solution given in (17). Specifically, we consider the exponential expression for the vertical x-layer

$$e^{-\frac{\sigma_x \cos\phi}{1+M\cos\phi}x}. \tag{26}$$

Since σ_x is always positive, the expression in (26) will be exponentially decaying only if

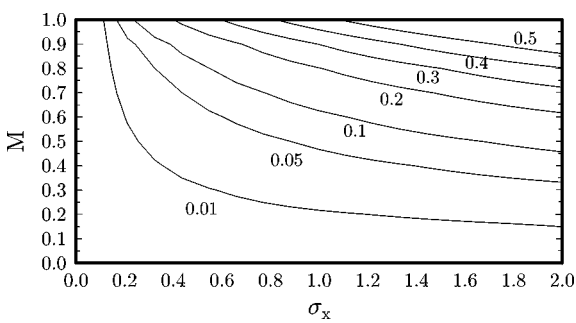

FIG. 2. Contours of maximum growth rate ω_i of the four roots computed numerically from dispersion relation (24) as a function of σ_x and Mach number M. Indicated are level values of ω_i. $\sigma_y = 0$, $|k_x| \le 5$ and $|k_y| \le 5$.

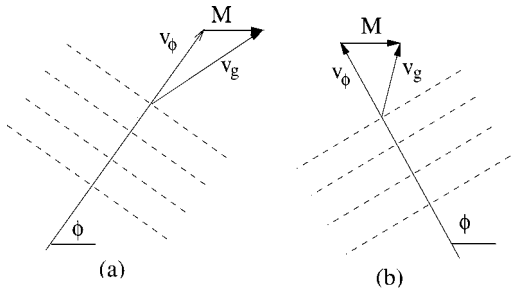

FIG. 3. A schematic drawing showing the relation between the wave-front normal vector $\mathbf{v}_\phi = (\cos\phi, \sin\phi)$ and the group velocity $\mathbf{v}_g$ of the acoustic wave in the presence of a mean flow of Mach number M. (a) A right-going wave with $\cos\phi > 0$; (b) a right-going wave with $\cos\phi < 0$.

the wave is

$$\text{right going} \quad \text{and} \quad \cos\phi > 0$$

or

$$\text{left going} \quad \text{and} \quad \cos\phi < 0,$$

where ϕ is the angle of the wave-front normal vector as defined in (5). Here, the direction of wave propagation is determined by the group velocity $\mathbf{v}_g$, in that a wave is right going or left going if the x-component of the group velocity is positive or negative, respectively. In the presence of a mean flow, however, as we will see below, the group velocity is not always in the same direction as that of the phase velocity and there now exist right-going waves with $\cos\phi < 0$.

For the acoustic waves in the Euler equations, the group velocity, by dispersion relation (3), is

$$\mathbf{v}_g = \left(\frac{\partial\omega}{\partial k_x}, \frac{\partial\omega}{\partial k_y}\right) = (M + \cos\phi, \sin\phi), \tag{27}$$

where ϕ is as defined in (5) (see, e.g., [26, 27]). Obviously, there may be right-going waves ($M + \cos\phi > 0$) with $\cos\phi < 0$, as illustrated in Fig. 3. For these waves, therefore, the wave amplitude actually grows exponentially after entering the PML domain, giving rise to the instability. The unstable angles, ϕ, are shown in Fig. 4.

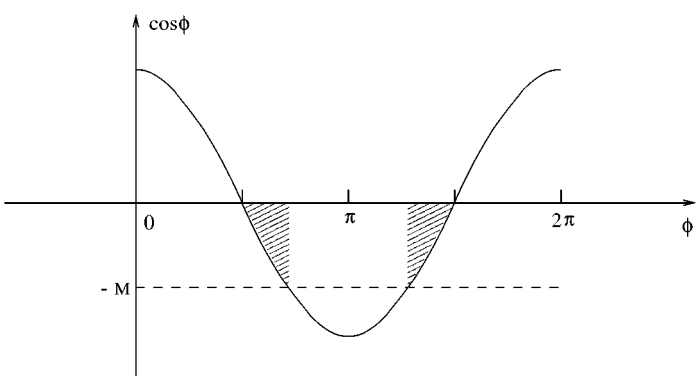

FIG. 4. Shaded are the angles of the acoustic waves that will be amplified when they enter the PML domain.

On the other hand, for the horizontal y-layers in which $\sigma_x = 0$, no instability will occur, since the y-component of the group velocity is in the same direction as that of the phase velocity. In addition, the vorticity and entropy waves do not concern us because they travel with the mean flow in the x-direction and will be decaying exponentially according to (18) and (19).

5. STABLE PML EQUATIONS

As we have seen in the previous section, the instability of Eqs. (21) and (22), or (10) and (11), is caused by the convective acoustic waves that have a positive group velocity but a negative phase velocity in the x-direction, i.e., a divergence in the group velocity and the phase velocity. Therefore, to construct stable PML equations, we first use a transformation so that in the transformed coordinates the acoustic waves become nonconvective and the group velocities of all linear waves are in the same direction as that of the phase velocities. We then apply the PML technique to the transformed equations.

Following similar transformations used in several previous works in dealing with the convective wave equation (see, e.g., [5, 16, 17, 28]), we introduce new variables $\bar{x}$, $\bar{y}$, and $\bar{t}$ as follows:

$$\bar{x} = x, \quad \bar{y} = \sqrt{1 - M^2}\, y, \quad \bar{t} = t + \frac{M}{1 - M^2} x. \tag{28}$$

The corresponding transformed wavenumbers and frequency are

$$\bar{k}_x = k_x + \frac{M}{1 - M^2}\omega, \quad \bar{k}_y = \frac{1}{\sqrt{1 - M^2}} k_y, \quad \bar{\omega} = \omega. \tag{29}$$

In the transformed variables, the Euler equation (1) is found to be

$$\left(\mathbf{I} + \frac{M}{1 - M^2}\mathbf{A}\right)\frac{\partial \mathbf{u}}{\partial \bar{t}} + \mathbf{A}\frac{\partial \mathbf{u}}{\partial \bar{x}} + \sqrt{1 - M^2}\,\mathbf{B}\frac{\partial \mathbf{u}}{\partial \bar{y}} = 0, \tag{30}$$

where $\mathbf{I}$ is the identity matrix. It also is easy to find that the dispersion relations for (30) in the transformed wavenumbers and frequency are

$$\frac{\bar{\omega}^2}{(1 - M^2)^2} - \bar{k}_x^2 - \bar{k}_y^2 = 0$$

for the acoustic waves and

$$\frac{\bar{\omega}}{1 - M^2} - M\bar{k}_x = 0$$

for the vorticity and entropy waves. As we can see, the acoustic waves are now nonconvective in the transformed variables and, further, the directions of propagation for the vorticity and entropy waves are unaltered. We note that transformation (28) is slightly different from those used in Refs. [5], [16], and [17] in that the frequency, or time derivative, is unchanged under the transformation. This is for the convenience of dealing with the auxiliary variable later.

Now, we apply the PML complex change of variables (15) to the transformed equation (30). In the frequency domain, we modify (30) to be

$$-i\omega\left(\mathbf{I}+\frac{M}{1-M^2}\mathbf{A}\right)\mathbf{u}+\frac{1}{1+\frac{i\sigma_x}{\bar{\omega}}}\mathbf{A}\frac{\partial\mathbf{u}}{\partial\bar{x}}+\sqrt{1-M^2}\frac{1}{1+\frac{i\sigma_y}{\bar{\omega}}}\mathbf{B}\frac{\partial\mathbf{u}}{\partial\bar{y}}=0. \tag{31}$$

After multiplying (31) by $(1+i\sigma_x/\bar{\omega})(1+i\sigma_y/\bar{\omega})$, we rewrite it back in the time domain,

$$\left(\mathbf{I}+\frac{M}{1-M^2}\mathbf{A}\right)\left[\frac{\partial\mathbf{u}}{\partial\bar{t}}+(\sigma_x+\sigma_y)\mathbf{u}+\sigma_x\sigma_y\mathbf{q}\right]+\mathbf{A}\frac{\partial\mathbf{u}}{\partial\bar{x}}+\sigma_y\mathbf{A}\frac{\partial\mathbf{q}}{\partial\bar{x}}$$
$$+\sqrt{1-M^2}\mathbf{B}\frac{\partial\mathbf{u}}{\partial\bar{y}}+\sigma_x\sqrt{1-M^2}\mathbf{B}\frac{\partial\mathbf{q}}{\partial\bar{y}}=0,$$

where $\mathbf{q}$ is the same as that given in (22). Finally, when expressed in the original variables x, y, and t, we get the new formulation of the PML equations,

$$\frac{\partial\mathbf{u}}{\partial t}+\mathbf{A}\frac{\partial\mathbf{u}}{\partial x}+\mathbf{B}\frac{\partial\mathbf{u}}{\partial y}+\sigma_y\mathbf{A}\frac{\partial\mathbf{q}}{\partial x}+\sigma_x\mathbf{B}\frac{\partial\mathbf{q}}{\partial y}+(\sigma_x+\sigma_y)\mathbf{u}$$
$$+\sigma_x\sigma_y\mathbf{q}+\frac{\sigma_x M}{1-M^2}\mathbf{A}(\mathbf{u}+\sigma_y\mathbf{q})=0, \tag{32}$$

$$\frac{\partial\mathbf{q}}{\partial t}=\mathbf{u}. \tag{33}$$

To show the stability of (32) and (33) (i.e., that there is no exponentially growing solution), we need to show only that the corresponding dispersion relations do not have any root ω with a positive imaginary part for any real values of wavenumbers k_x and k_y. It is easy to show that the dispersion relations for (32) and (33) can be found, equivalently, by replacing k_x and k_y in (3) and (4) with

$$k_x\to\frac{1}{1+\frac{i\sigma_x}{\omega}}\left(k_x+\frac{M}{1-M^2}\omega\right)-\frac{M}{1-M^2}\omega,\quad k_y\to\frac{k_y}{1+\frac{i\sigma_y}{\omega}}, \tag{34}$$

and we readily get

$$\frac{(\omega+i\sigma_x)^2(\omega+i\sigma_y)^2}{(1-M^2)^2}-(\omega+i\sigma_y)^2\left(k_x+\frac{M}{1-M^2}\omega\right)^2-\frac{1}{1-M^2}(\omega+i\sigma_x)^2k_y^2=0 \tag{35}$$

for the acoustics waves and

$$\omega+\frac{i\sigma_x}{1-M^2}-Mk_x=0 \tag{36}$$

for the vorticity and entropy waves. Actually, Eqs. (32) and (33) should have eight roots for ω. The two additional roots for ω are found to be $\omega=-i\sigma_y$ with a multiplicity of 2.

Clearly, (36) is stable. The stability of (35) can be shown by symbolic calculations, and the details are given in Appendix 1. A specific case of $M=0.9$, $\sigma_x=1.5$, and $\sigma_y=0$ is shown numerically in Fig. 5 in which the contours of maximum ω_i as a function of k_x and k_y, solved numerically from (35), are plotted. All the contours are in dashed lines, which

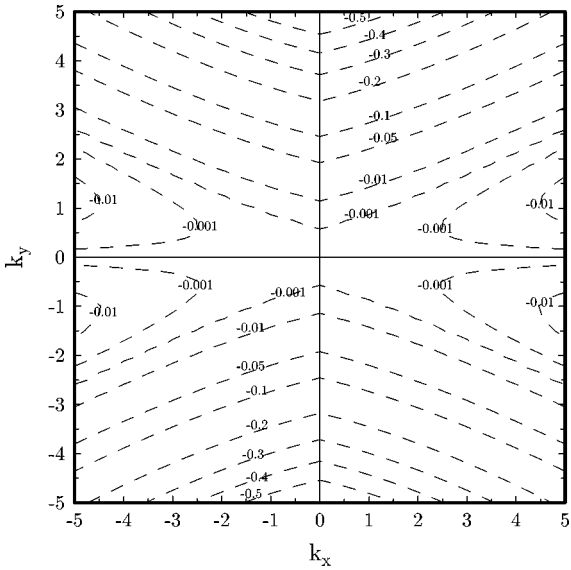

FIG. 5. Contours of maximum ω_i, imaginary part of ω, of the four roots solved numerically from (35). $M = 0.9$, $\sigma_x = 1.5$ and $\sigma_y = 0$. Indicated are the contour levels.

means that the values of ω_i are all negative. Therefore, (35) will not admit exponentially growing solutions.

It is also straightforward to find that the plane wave solutions to (32) and (33) are

$$\begin{pmatrix}\rho\\ u\\ v\\ p\end{pmatrix} = A\begin{pmatrix}1\\ \cos\phi\\ \sin\phi\\ 1\end{pmatrix}\exp\Bigg(\frac{i\omega\cos\phi}{1+M\cos\phi}x - \frac{\sigma_x(M+\cos\phi)}{(1-M^2)(1+M\cos\phi)}x + \frac{i\omega\sin\phi}{1+M\cos\phi}y - \frac{\sigma_y\sin\phi}{1+M\cos\phi}y - i\omega t\Bigg) \quad \text{(acoustic)}, \tag{37}$$

$$\begin{pmatrix}\rho\\ u\\ v\\ p\end{pmatrix} = B\begin{pmatrix}0\\ -\sin\psi\\ \cos\psi\\ 0\end{pmatrix}\exp\Bigg(\frac{i\omega}{M}x - \frac{\sigma_x}{(1-M^2)M}x + \frac{i\omega\tan\psi}{M}y - \frac{\sigma_y\tan\psi}{M}y - i\omega t\Bigg) \quad \text{(vorticity)}, \tag{38}$$

$$\begin{pmatrix}\rho\\ u\\ v\\ p\end{pmatrix} = C\begin{pmatrix}1\\ 0\\ 0\\ 0\end{pmatrix}\exp\Bigg(\frac{i\omega}{M}x - \frac{\sigma_x}{(1-M^2)M}x + \frac{i\omega\tan\chi}{M}y - \frac{\sigma_y\tan\chi}{M}y - i\omega t\Bigg) \quad \text{(entropy)}, \tag{39}$$

where ϕ, ψ and χ are, again, the angles of the wave-front normal vectors. From (37)–(39), we can show easily that the solutions are perfectly matched at any vertical interface

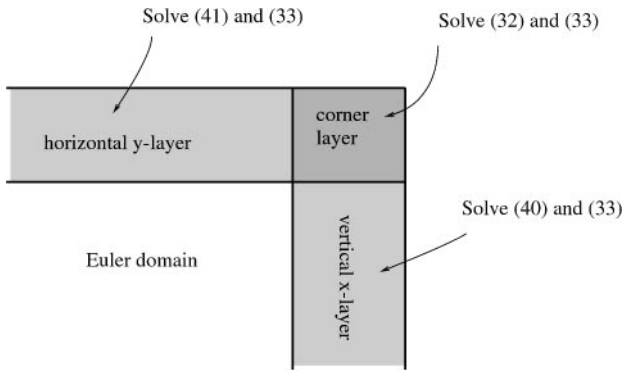

FIG. 6. An illustration of simplified PML equations for different layers.

where σ_y is the same on both sides of the interface, and on any horizontal interface where σ_x is the same on both sides [14]. This includes the interfaces between the Euler domain and a PML domain as well as the interfaces between two PML domains, such as those at the corner layers. When compared with (17)–(19), the acoustic waves now are absorbed correctly according to the group velocity. In addition, the absorption rate in the x-direction is increased by a factor of $1/(1-M^2)$. This means that the absorption rate in the x-direction will be larger than that in the y-direction if the values of absorption coefficients are the same.

We note that at a vertical x-layer or horizontal y-layer, one of the absorption coefficients is zero, and accordingly, a simpler form of (32) results. Specifically, we have two simplified equations. At a vertical x-layer ($\sigma_y = 0$), we solve

$$\frac{\partial \mathbf{u}}{\partial t} + \mathbf{A}\frac{\partial \mathbf{u}}{\partial x} + \mathbf{B}\frac{\partial \mathbf{u}}{\partial y} + \sigma_x \mathbf{B}\frac{\partial \mathbf{q}}{\partial y} + \sigma_x \mathbf{u} + \frac{\sigma_x M}{1-M^2}\mathbf{A}\mathbf{u} = 0. \tag{40}$$

At a horizontal y-layer ($\sigma_x = 0$), we solve

$$\frac{\partial \mathbf{u}}{\partial t} + \mathbf{A}\frac{\partial \mathbf{u}}{\partial x} + \mathbf{B}\frac{\partial \mathbf{u}}{\partial y} + \sigma_y \mathbf{A}\frac{\partial \mathbf{q}}{\partial x} + \sigma_y \mathbf{u} = 0. \tag{41}$$

In both cases, the equation for $\mathbf{q}$ is (33). At a corner layer, of course, the full version of (32) and (33) should be used. This situation is depicted in Fig. 6.

6. WELL-POSEDNESS

We now consider the well-posedness of the proposed stable PML equations (32) and (33). For a system of hyperbolic equations in multidimensions, in general, stability alone does not ensure well-posedness [29, 30]. For convenience of discussion, we write the equations in the block matrix form

$$\frac{\partial}{\partial t}\begin{pmatrix}\mathbf{u}\\ \mathbf{q}\end{pmatrix} + \begin{pmatrix}\mathbf{A} & \sigma_y\mathbf{A}\\ 0 & 0\end{pmatrix}\frac{\partial}{\partial x}\begin{pmatrix}\mathbf{u}\\ \mathbf{q}\end{pmatrix} + \begin{pmatrix}\mathbf{B} & \sigma_x\mathbf{B}\\ 0 & 0\end{pmatrix}\frac{\partial}{\partial y}\begin{pmatrix}\mathbf{u}\\ \mathbf{q}\end{pmatrix} + \mathbf{Q}\begin{pmatrix}\mathbf{u}\\ \mathbf{q}\end{pmatrix} = 0, \tag{42}$$

where

$$\mathbf{Q} = \begin{pmatrix} (\sigma_x + \sigma_y)\mathbf{I} + \sigma_x \frac{M}{1-M^2}\mathbf{A} & \sigma_x\sigma_y\left(\mathbf{I} + \frac{M}{1-M^2}\mathbf{A}\right) \\ -\mathbf{I} & 0 \end{pmatrix}$$

and define

$$\mathbf{P} = k_x \begin{pmatrix} \mathbf{A} & \sigma_y\mathbf{A} \\ 0 & 0 \end{pmatrix} + k_y \begin{pmatrix} \mathbf{B} & \sigma_x\mathbf{B} \\ 0 & 0 \end{pmatrix} = \begin{pmatrix} k_x\mathbf{A} + k_y\mathbf{B} & k_x\sigma_y\mathbf{A} + k_y\sigma_x\mathbf{B} \\ 0 & 0 \end{pmatrix}. \tag{43}$$

We first show that $\mathbf{P}$ has all real eigenvalues and a complete set of eigenvectors. Let

$$\begin{pmatrix} k_x\mathbf{A} + k_y\mathbf{B} & k_x\sigma_y\mathbf{A} + k_y\sigma_x\mathbf{B} \\ 0 & 0 \end{pmatrix} \begin{pmatrix} \mathbf{e_u} \\ \mathbf{e_q} \end{pmatrix} = \lambda \begin{pmatrix} \mathbf{e_u} \\ \mathbf{e_q} \end{pmatrix}.$$

We get

$$(k_x\mathbf{A} + k_y\mathbf{B})\mathbf{e_u} + (k_x\sigma_y\mathbf{A} + k_y\sigma_x\mathbf{B})\mathbf{e_q} = \lambda\mathbf{e_u},$$
$$0 = \lambda\mathbf{e_q}.$$

Clearly, there are two subsets of eigenvalues and eigenvectors, namely, those of $k_x\mathbf{A} + k_y\mathbf{B}$ (the same as that of the Euler equations) with $\mathbf{e_q} = 0$ and those from $\lambda = 0$ (multiplicity 4) with $\mathbf{e_q}$ being arbitrary and $\mathbf{e_u} = -(k_x\mathbf{A} + k_y\mathbf{B})^{-1}(k_x\sigma_y\mathbf{A} + k_y\sigma_x\mathbf{B})\mathbf{e_q}$.

To study the well-posedness of (32) and (33), it suffices to consider the equations without the nonderivative terms [29, 30]. This leads to the initial value problem

$$\frac{\partial\mathbf{u}}{\partial t} + \mathbf{A}\frac{\partial\mathbf{u}}{\partial x} + \mathbf{B}\frac{\partial\mathbf{u}}{\partial y} + \sigma_y\mathbf{A}\frac{\partial\mathbf{q}}{\partial x} + \sigma_x\mathbf{B}\frac{\partial\mathbf{q}}{\partial y} = 0, \tag{44}$$

$$\frac{\partial\mathbf{q}}{\partial t} = 0, \tag{45}$$

with initial conditions

$$\mathbf{u}(x, y, 0) = \mathbf{u}_0(x, y), \quad \mathbf{q}(x, y, 0) = \mathbf{q}_0(x, y). \tag{46}$$

Immediately from (45) we have

$$\mathbf{q}(x, y, t) = \mathbf{q}_0(x, y). \tag{47}$$

Applying a Fourier transform in space to (44), we get

$$\frac{\partial\hat{\mathbf{u}}}{\partial t} + i(k_x\mathbf{A} + k_y\mathbf{B})\hat{\mathbf{u}} + i(k_x\sigma_y\mathbf{A} + k_y\sigma_x\mathbf{B})\hat{\mathbf{q}}_0 = 0, \tag{48}$$

where

$$\hat{\mathbf{u}}(k_x, k_y, t) = \frac{1}{2\pi}\int_{-\infty}^{\infty}\int_{-\infty}^{\infty}\mathbf{u}(x, y, t)e^{-i(k_x x + k_y y)}\,dx\,dy$$

and likewise for $\hat{\mathbf{q}}$. Further, we note that matrix $k_x\mathbf{A} + k_y\mathbf{B}$ can be uniformly diagonalized. Specifically, we have

$$\mathbf{E}(k_x\mathbf{A} + k_y\mathbf{B})\mathbf{E}^{-1} = \Lambda, \tag{49}$$

where

$$\Lambda = \begin{pmatrix} Mk_x & 0 & 0 & 0 \\ 0 & Mk_x & 0 & 0 \\ 0 & 0 & Mk_x + k & 0 \\ 0 & 0 & 0 & Mk_x - k \end{pmatrix}$$

and

$$\mathbf{E} = \begin{pmatrix} 1 & 0 & 0 & -1 \\ 0 & -\frac{k_y}{k} & \frac{k_x}{k} & 0 \\ 0 & \frac{k_x}{2k} & \frac{k_y}{2k} & \frac{1}{2} \\ 0 & -\frac{k_x}{2k} & -\frac{k_y}{2k} & \frac{1}{2} \end{pmatrix}, \quad \mathbf{E}^{-1} = \begin{pmatrix} 1 & 0 & 1 & 1 \\ 0 & -\frac{k_y}{k} & \frac{k_x}{k} & -\frac{k_x}{k} \\ 0 & \frac{k_x}{k} & \frac{k_y}{k} & -\frac{k_y}{k} \\ 0 & 0 & 1 & 1 \end{pmatrix}$$

in which $k = \sqrt{k_x^2 + k_y^2}$. Both $\mathbf{E}$ and $\mathbf{E}^{-1}$ are uniformly bounded for all values of k_x and k_y.

Utilizing (49), it is easy to find that the solution for $\hat{\mathbf{u}}$ is

$$\hat{\mathbf{u}} = \mathbf{E}^{-1} e^{-i\Lambda t} \mathbf{E} \hat{\mathbf{u}}_0 - \mathbf{E}^{-1}(\mathbf{I} - e^{-i\Lambda t})\Lambda^{-1}\mathbf{E}(k_x\sigma_y\mathbf{A} + k_y\sigma_x\mathbf{B})\hat{\mathbf{q}}_0. \tag{50}$$

For well-posedness, $\hat{\mathbf{u}}$ needs to be bounded for all values of k_x and k_y and dependent continuously on the initial conditions. Since both $\mathbf{E}$ and $\mathbf{E}^{-1}$ are bounded, the first term in (50) is bounded. Further, since we have (by (64) and (65) in Appendix 2)

$$\|k_x \Lambda^{-1}\| \le C_0 \tag{51}$$

and

$$\|(\mathbf{I} - e^{-i\Lambda t})\Lambda^{-1}\| < t, \tag{52}$$

where C_0 is a constant independent of k_x and k_y, we get

$$\begin{aligned} \|\hat{\mathbf{u}}\| \le{}& \|\mathbf{E}^{-1}\| \cdot \|\mathbf{E}\| \cdot \|\hat{\mathbf{u}}_0\| + 2C_0\sigma_y \|\mathbf{E}^{-1}\| \cdot \|\mathbf{E}\| \cdot \|\mathbf{A}\| \cdot \|\hat{\mathbf{q}}_0\| \\ &+ \sigma_x t|k_y| \cdot \|\mathbf{E}^{-1}\| \cdot \|\mathbf{E}\| \cdot \|\mathbf{B}\| \cdot \|\hat{\mathbf{q}}_0\|. \end{aligned} \tag{53}$$

Here $\|\cdot\|$ denotes the L_2 norm.

From (53), we easily see that when $\sigma_x = 0$ (i.e., in horizontal y-layers), the last term in (53) vanishes and $\hat{\mathbf{u}}$ is uniformly bounded independent of k_x and k_y. This means that (32) and (33) are well-posed. On the other hand, when $\sigma_x \neq 0$ (in vertical x-layers and corner layers), the solution may depend on the first derivative of the initial data, which renders the equations only weakly well-posed.

One concern for a weakly well-posed problem is that it may become ill-posed under certain low-order perturbations. Although it remains to be seen whether such a perturbation exists for (32) and (33), we shall show next that the PML equations (32) and (33) can be made symmetrizable and, thus, strongly well-posed, with only a slight modification.

Consider a modified version of Eqs. (32) and (33) that changes only the equation for $\mathbf{q}$,

$$\frac{\partial \mathbf{u}}{\partial t} + \mathbf{A}\frac{\partial \mathbf{u}}{\partial x} + \mathbf{B}\frac{\partial \mathbf{u}}{\partial y} + \sigma_y \mathbf{A}\frac{\partial \mathbf{q}}{\partial x} + \sigma_x \mathbf{B}\frac{\partial \mathbf{q}}{\partial y} + (\sigma_x + \sigma_y)\mathbf{u} + \sigma_x \sigma_y \mathbf{q} + \frac{\sigma_x M}{1 - M^2}\mathbf{A}(\mathbf{u} + \sigma_y \mathbf{q}) = 0, \tag{54}$$

$$\frac{\partial \mathbf{q}}{\partial t} + \epsilon \sigma_y \mathbf{A}\frac{\partial \mathbf{u}}{\partial x} + \epsilon \sigma_x \mathbf{B}\frac{\partial \mathbf{u}}{\partial y} - \mathbf{u} = 0, \tag{55}$$

where ϵ is any small positive number. When written in block matrix form, (54) and (55) become

$$\frac{\partial}{\partial t}\begin{pmatrix}\mathbf{u}\\ \mathbf{q}\end{pmatrix} + \begin{pmatrix}\mathbf{A} & \sigma_y \mathbf{A}\\ \epsilon \sigma_y \mathbf{A} & 0\end{pmatrix}\frac{\partial}{\partial x}\begin{pmatrix}\mathbf{u}\\ \mathbf{q}\end{pmatrix} + \begin{pmatrix}\mathbf{B} & \sigma_x \mathbf{B}\\ \epsilon \sigma_x \mathbf{B} & 0\end{pmatrix}\frac{\partial}{\partial y}\begin{pmatrix}\mathbf{u}\\ \mathbf{q}\end{pmatrix} + \mathbf{Q}\begin{pmatrix}\mathbf{u}\\ \mathbf{q}\end{pmatrix} = 0. \tag{56}$$

Equation (56) is now symmetrizable. To show this, we note the fact that, for the Euler equation (1), matrices $\mathbf{A}$ and $\mathbf{B}$ can be simultaneously symmetrized. That is, there is a matrix $\mathbf{S}$ such that

$$\mathbf{S}\mathbf{A}\mathbf{S}^{-1} = \tilde{\mathbf{A}}, \qquad \mathbf{S}\mathbf{B}\mathbf{S}^{-1} = \tilde{\mathbf{B}},$$

where both $\tilde{\mathbf{A}}$ and $\tilde{\mathbf{B}}$ are symmetric matrices. Specifically, for the $\mathbf{A}$ and $\mathbf{B}$ given in (2), we have

$$\mathbf{S} = \begin{pmatrix} 1 & 0 & 0 & -1 \\ 0 & 0 & \frac{\sqrt{2}}{2} & 0 \\ 0 & \frac{1}{2} & 0 & \frac{1}{2} \\ 0 & -\frac{1}{2} & 0 & \frac{1}{2} \end{pmatrix}, \quad \tilde{\mathbf{A}} = \begin{pmatrix} M & 0 & 0 & 0 \\ 0 & M & 0 & 0 \\ 0 & 0 & M+1 & 0 \\ 0 & 0 & 0 & M-1 \end{pmatrix},$$

$$\tilde{\mathbf{B}} = \begin{pmatrix} 0 & 0 & 0 & 0 \\ 0 & 0 & \frac{\sqrt{2}}{2} & \frac{\sqrt{2}}{2} \\ 0 & \frac{\sqrt{2}}{2} & 0 & 0 \\ 0 & \frac{\sqrt{2}}{2} & 0 & 0 \end{pmatrix}.$$

Now for (56), let

$$\mathbf{T} = \begin{pmatrix} \mathbf{S} & 0 \\ 0 & \frac{1}{\sqrt{\epsilon}}\mathbf{S} \end{pmatrix}.$$

It is straightforward to verify that

$$\mathbf{T}\begin{pmatrix}\mathbf{A} & \sigma_y \mathbf{A}\\ \epsilon \sigma_y \mathbf{A} & 0\end{pmatrix}\mathbf{T}^{-1} = \begin{pmatrix}\tilde{\mathbf{A}} & \sqrt{\epsilon}\sigma_y \tilde{\mathbf{A}}\\ \sqrt{\epsilon}\sigma_y \tilde{\mathbf{A}} & 0\end{pmatrix}$$

and

$$\mathbf{T}\begin{pmatrix}\mathbf{B} & \sigma_x \mathbf{B}\\ \epsilon \sigma_x \mathbf{B} & 0\end{pmatrix}\mathbf{T}^{-1} = \begin{pmatrix}\tilde{\mathbf{B}} & \sqrt{\epsilon}\sigma_x \tilde{\mathbf{B}}\\ \sqrt{\epsilon}\sigma_x \tilde{\mathbf{B}} & 0\end{pmatrix}.$$

Both are now symmetric matrices. Therefore, (56), or (54) and (55), are symmetrizable and, thus, strongly well-posed [30].

Although the introduction of a small parameter ϵ in (55) formally alters the perfectly matched status of the equations, its impact on accuracy in actual computations is expected to be negligible as the value of ϵ can be arbitrarily small. Indeed, as we will see in Section 7, numerical results show very little difference between the solutions obtained using (32) and (33) and those using (54) and (55) for a value of $\epsilon = 0.005$ or smaller. In view of this, the stable version (32) and (33) is recommended for most practical computations, since it is simpler and, thus, computationally less costly. The symmetrizable version given in (54) and (55) is suggested if a symmetrizable hyperbolic system is preferred or necessary for the application.

7. NUMERICAL EXAMPLES

We present two numerical examples to demonstrate the stability and the effectiveness of the PML equations proposed in this paper as an absorbing boundary condition. Unless noted otherwise, the PML equations used in the computations are those given in (32) and (33). Both the Euler equation and PML equations are solved numerically by a finite difference scheme. Specifically, the spatial derivatives are discretized by a fourth-order, seven point central difference scheme given in [8] (the dispersion-relation-preserving scheme), combined with a five point boundary-closure scheme given in [31]. The time integration is carried out by a fourth-order Runge–Kutta scheme that has been optimized for minimal dissipation and dispersion errors [32] (the LDDRK56 scheme). Further details of the scheme can be found in [15] and [33]. As mentioned in Section 3, the auxiliary variable $\mathbf{q}$ is only introduced in the PML domains and is neither computed nor stored in the interior Euler domain. To verify stability, no numerical filtering or damping is used in all the computations reported here. Indeed, numerical results show no instability.

Since a wide stencil is used in the finite difference scheme, the absorption coefficients are varied gradually inside a PML domain. The variations of absorption coefficients used in the computations are

$$\sigma_x = \sigma_m(1 - M^2)\left|\frac{x - x_l}{D}\right|^\beta, \quad \sigma_y = \sigma_m\left|\frac{y - y_l}{D}\right|^\beta, \tag{57}$$

where x_l or y_l denotes the location where the PML domain starts, and D is the width of the PML domain. A factor of $1 - M^2$ has been included in σ_x so that the absorption rates remain the same in both the x and y directions for the reason stated in Section 5. Values of $\sigma_m \Delta x = 2$, where Δx is the grid size, and $\beta = 2$ are used for all the results.

At the end of the PML domain, no special boundary conditions are needed except those that are necessary to maintain the numerical stability of the scheme. According to the characteristics of (32) and (33), for a subsonic mean flow, we should specify three boundary conditions at the left side of the computational domain and one boundary condition each at the other three sides. For the results reported here, we apply these simple boundary conditions at end points of the PML domains,

$$\text{at } x = X_{max}, y = Y_{min} \quad \text{and} \quad y = Y_{max} : p = 0,$$
$$\text{at inflow } x = X_{min} : p = \rho = v = 0,$$

in which $[X_{min}, X_{max}] \times [Y_{min}, Y_{max}]$ denotes the entire computational domain as indicated in Fig. 1. Other forms of characteristics-based boundary conditions are equally applicable. Alternatively, it is also possible to apply periodic boundary conditions since the numerical solution decays exponentially toward all the boundaries.

7.1. Propagation of Gaussian Pulses

In the first example, the Euler domain is initialized with acoustic, vorticity, and entropy pulses, with amplitudes A_0, B_0, and C_0, respectively, as follows:

$$\rho = A_0 \exp\left[-(\ln 2)\frac{(x+20)^2+y^2}{16}\right] + C_0 \exp\left[-(\ln 2)\frac{(x-20)^2+y^2}{16}\right],$$

$$u = B_0 y \exp\left[-(\ln 2)\frac{(x-20)^2+y^2}{16}\right],$$

$$v = -B_0(x-20) \exp\left[-(\ln 2)\frac{(x-20)^2+y^2}{16}\right],$$

$$p = A_0 \exp\left[-(\ln 2)\frac{(x+20)^2+y^2}{16}\right].$$

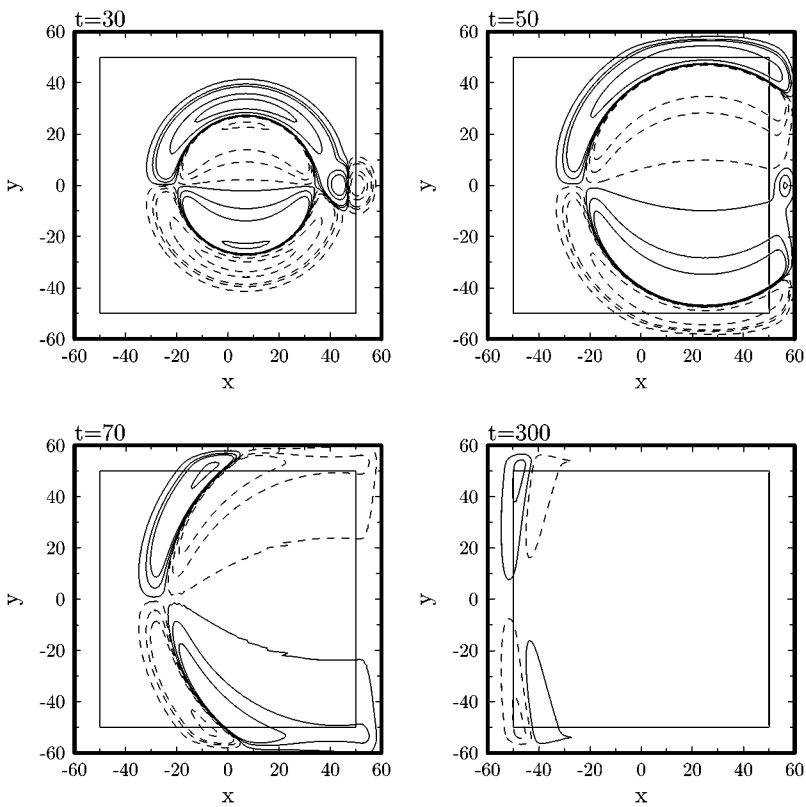

FIG. 7. Contours of the v velocity component at levels ± 0.1, ± 0.05, ± 0.01, ± 0.005, and ± 0.001. Four graphs correspond to time $t = 30$, 50, 70, and 300 as indicated. $M = 0.9$, $D = 10\Delta x$.

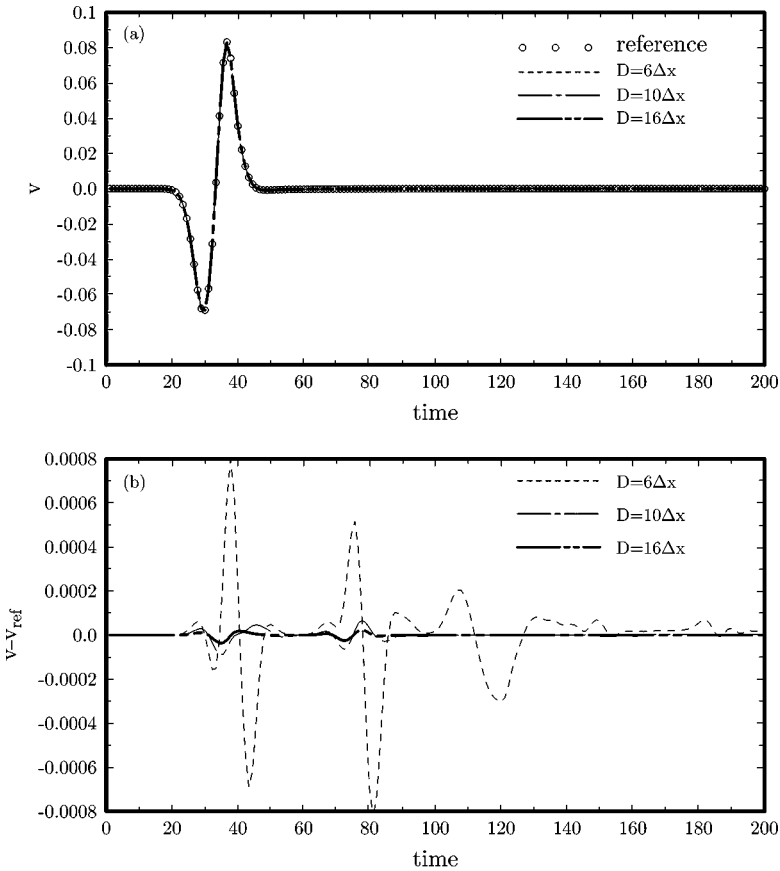

FIG. 8. (a) The v velocity component as a function of time at point $(x, y) = (50, 5)$. (b) The difference between the numerical and the reference solutions.

We simulate the propagation of these pulses in a mean flow of Mach number $M = 0.9$. The amplitudes of pulses are $A_0 = B_0 = C_0 = 1$. The Euler domain is $[-50, 50] \times [-50, 50]$ and the PML domains extend further with a fixed number of grid points. A uniform grid of $\Delta x = \Delta y = 1$ has been used with a time step $\Delta t = 0.55$.

In Fig. 7, we show the v-velocity contours at time $t = 30, 50, 70,$ and 300. For this calculation, the PML domains are 10 points in width; i.e., $D = 10\Delta x$. The contour plots show the exponential decaying of the solution inside the PML domains with no visible reflection. In Fig. 8a, the time history of v at a location on the interface of the Euler and a PML domain, $(x, y) = (50, 5)$, is plotted. The graph includes results from three calculations for $D = 6\Delta x, 10\Delta x$, and $16\Delta x$, respectively. Also plotted in Fig. 8a is a reference solution which is calculated separately by using a larger computational domain so that it is not affected by the boundary conditions. All three cases show very little error on the scale of the graph. In Fig. 8b, the differences between the numerical and the reference solutions are plotted. The reflection errors are indeed very small, especially for $D = 10\Delta x$ and $16\Delta x$. To further assess the accuracy and effectiveness of the PML equations, we plot the maximum difference between the numerical and the reference solutions along all four interfaces, namely, $x = \pm 50$ and $y = \pm 50$, in Fig. 9. We see that the reflection error reduces with the increase of D. Clearly, the PML works very well in absorbing all three types of linear waves.

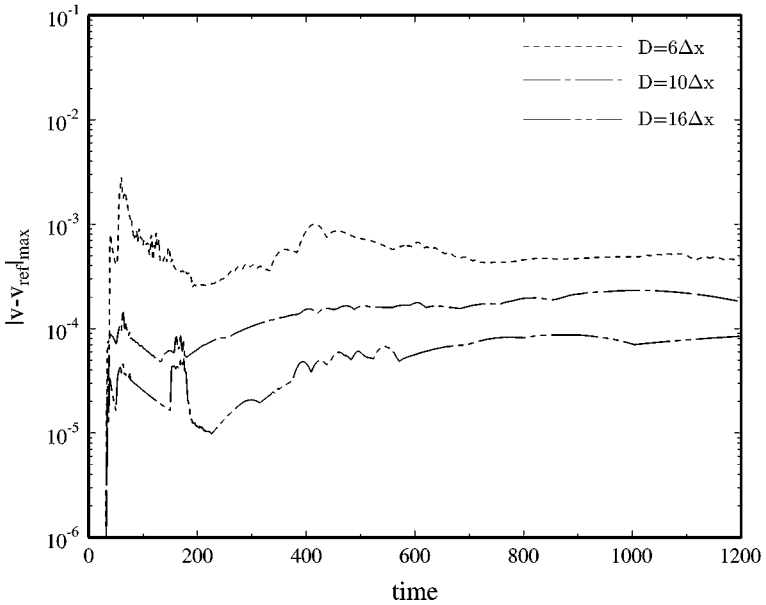

FIG. 9. Maximum difference between the numerical and the reference solutions along four interfaces at $x = \pm 50$ and $y \pm 50$.

7.2. Periodic Source

In the second example, we solve the Euler equations with the following source term added to the equation for the pressure:

$$S(x, y, t) = \sin(\Omega t) \exp\left[-(\ln 2)\frac{(x+20)^2 + y^2}{9}\right].$$

The frequency of the source is $\Omega = 0.03\pi$ and the mean-flow Mach number is $M = 0.8$. Because of the mean flow, the acoustic wave has a larger wavelength at the downstream boundary than at the upstream boundary. We use this example to show that PML equations are equally effective for long and short waves. The Euler domain is $[-100, 100] \times [-100, 100]$. The source is located at $(x, y) = (-20, 0)$. Figure 10 shows the pressure contours of the numerical solution at $t = 600$. The PML domains for this calculation have a width $D = 10\Delta x$. The calculated pressure as a function of time at two chosen locations, $(x, y) = (100, 10)$ and $(-100, 10)$, is plotted in Fig. 11. The differences between the numerical and the reference solutions are plotted in Fig. 12. Again, excellent agreements are observed. These two examples show that the proposed PML equations are stable and very accurate and effective as an absorbing boundary condition.

7.3. Results of the Symmetrizable Version

In this section, we show numerical results obtained using the symmetrizable PML equations (54) and (55). The same calculations presented in the first example are repeated. The reflection errors are shown in Fig. 13 for three calculations made with a PML domain width $D = 10\Delta x$ and $\epsilon = 0.001$, 0.005, and 0.01, respectively. Compared with the numerical results in Fig. 9 obtained in Section 7.1, we see very little difference for cases with $\epsilon = 0.001$

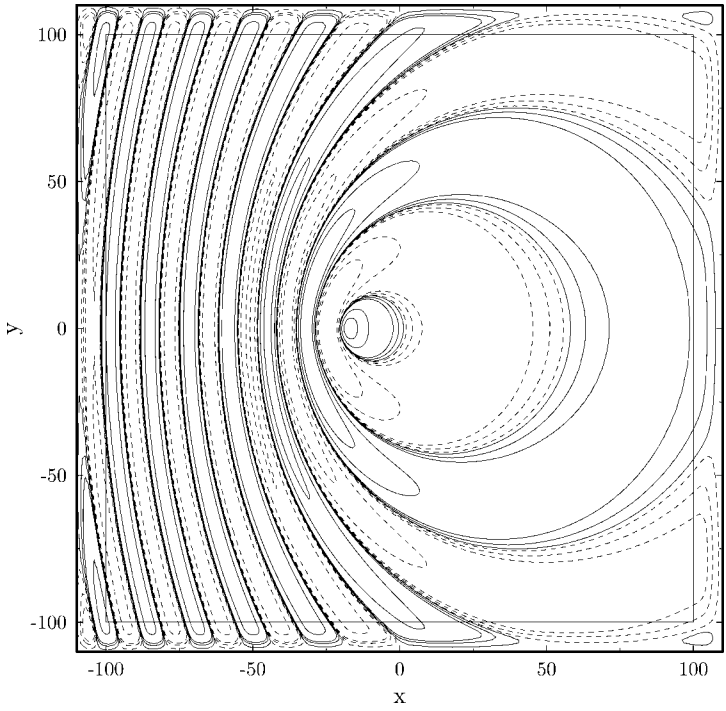

FIG. 10. Contours of the pressure p at levels $\pm 0.1, \pm 0.05, \pm 0.01, \pm 0.005$, and ± 0.001. $M = 0.8$, $D = 10\Delta x$. $t = 600$.

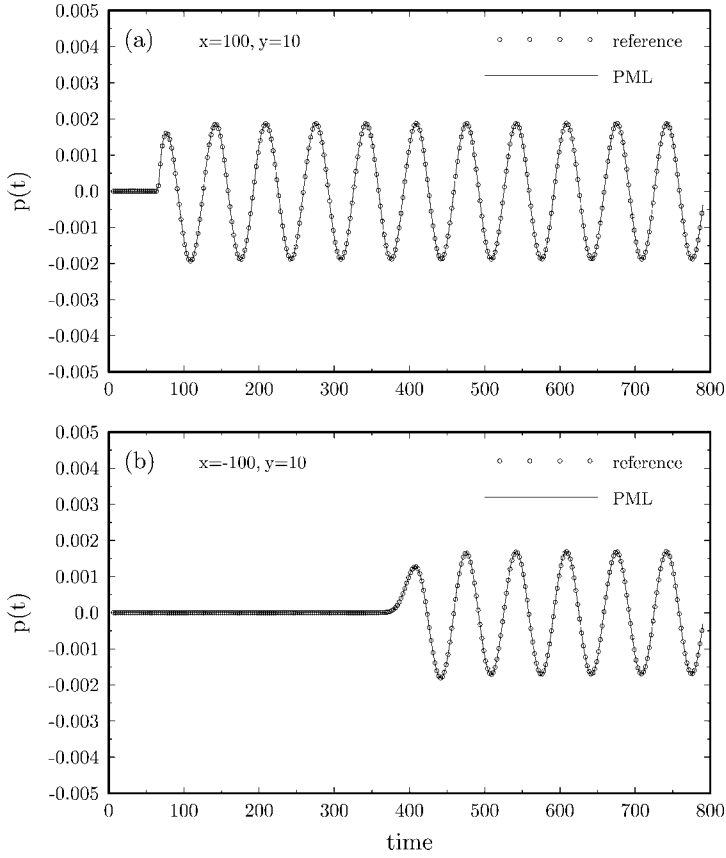

FIG. 11. Pressure as a function of time at two selected points. $M = 0.8$, $D = 10\Delta x$.

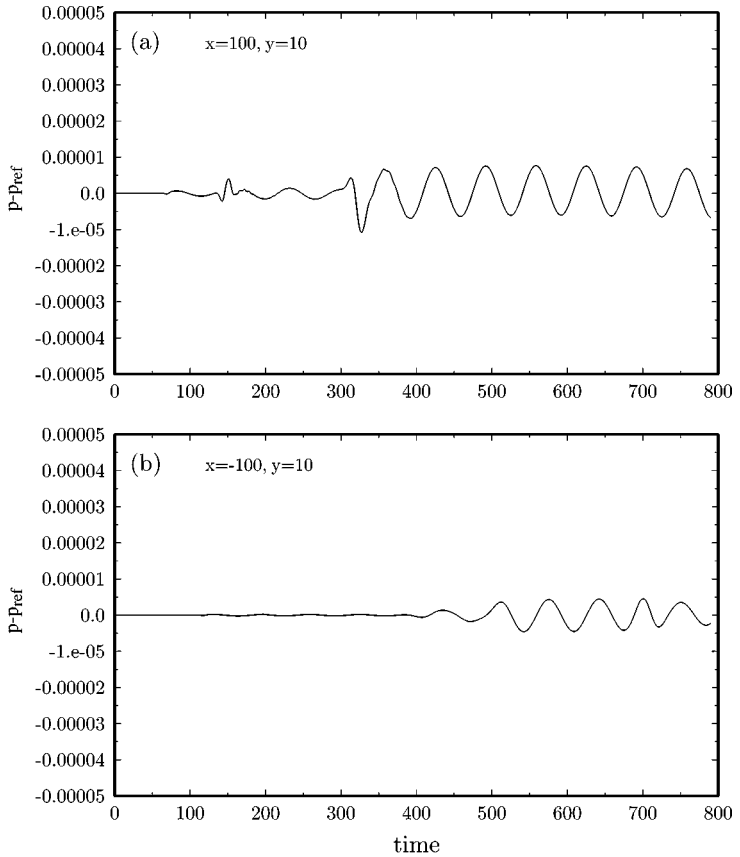

FIG. 12. Differences between the numerical and the reference solutions shown in Fig. 11.

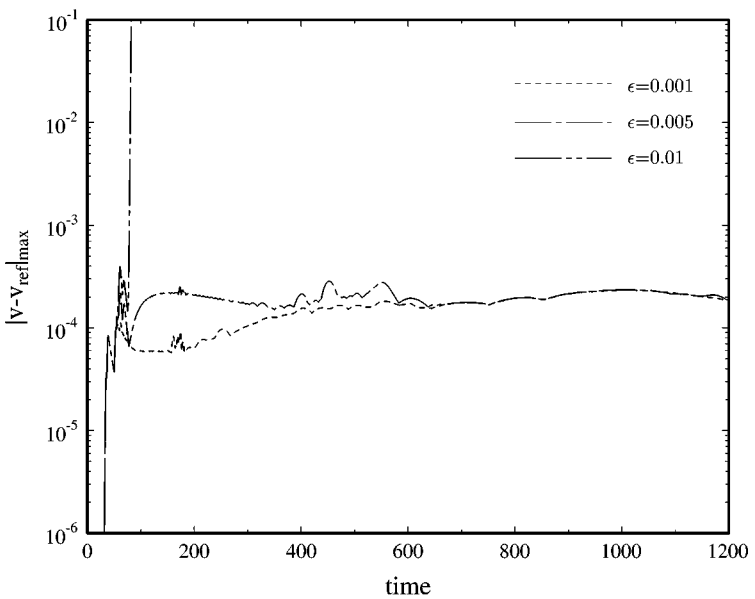

FIG. 13. Maximum difference between the numerical and the reference solutions along four interfaces at $x = \pm 50$ and $y \pm 50$. The PML equations used are those given in (54) and (55) with the value of ϵ as indicated.

and 0.005. A value of $\epsilon = 0.01$, however, produced unstable solution, since well-posedness does not exclude the situation where the solution could grow at a bounded finite rate [29, 30]. This should not be a problem in practical computations since ϵ can be taken to be an arbitrarily small number. Therefore, as these calculations have shown, the use of the symmetrizable PML equations (54) and (55) will not affect the accuracy.

8. CONCLUDING REMARKS

We have presented a stable PML formulation for the linearized Euler equations with a uniform mean flow. Numerical examples show that the proposed PML equations are very accurate and effective as a nonreflecting boundary condition for open-domain problems. For most practical computations, the stable version given in (32) and (33) is suggested because it is simpler than the symmetrizable version in (54) and (55) and, thus, computationally more efficient. Of course, for applications where a symmetric hyperbolic system is preferred or necessary, the symmetrizable version given in (54) and (55) can be readily used.

Compared with the author's earlier formulation [14], the present formulation does not need the application of numerical filtering or damping for the purpose of maintaining numerical stability. Moreover, the use of unsplit variables should better facilitate its implementation in many numerical schemes. Compared with the PML formulation given in [16], the present formulation appears to be simpler and, thus, is easier for its numerical implementation. The current formulation can also be extended to the Euler equations with a nonuniform mean flow. This will be reported in future work.

APPENDIX 1 : STABILITY OF EQUATION (35)

In this appendix, we show that all solutions to the dispersion relation (35) are stable.

We first show the stability of (35) in the transformed coordinates defined in (28). The corresponding dispersion relation in the transformed wavenumbers and frequency is

$$(\bar{\omega} + i\sigma_x)^2(\bar{\omega} + i\sigma_y)^2 - \beta^2\bar{k}_x^2(\bar{\omega} + i\sigma_y)^2 - \beta^2\bar{k}_y^2(\bar{\omega} + i\sigma_x)^2 = 0, \tag{58}$$

where $\beta = 1 - M^2$. Let

$$\bar{\omega} = \Omega + i\delta, \tag{59}$$

where we assume that both Ω and δ are real and $\delta > 0$. By substituting (59) into (58) we get

$$\Omega^4 - (\beta^2\bar{k}^2 + \tilde{\sigma}^2 + 4\tilde{\sigma}_{xy})\Omega^2 + \beta^2\bar{k}_x^2\tilde{\sigma}_y^2 + \beta^2\bar{k}_y^2\tilde{\sigma}_x^2 + \tilde{\sigma}_{xy}^2 = 0 \tag{60}$$

for the real part and

$$2(\tilde{\sigma}_x + \tilde{\sigma}_y)\Omega^3 - 2\left[\beta^2\bar{k}_x^2\tilde{\sigma}_y + \beta^2\bar{k}_y^2\tilde{\sigma}_x + (\tilde{\sigma}_x + \tilde{\sigma}_y)\tilde{\sigma}_{xy}\right]\Omega = 0 \tag{61}$$

for the imaginary part. For brevity, we use substitutions $\tilde{\sigma}_x = \sigma_x + \delta$, $\tilde{\sigma}_y = \sigma_y + \delta$, $\bar{k}^2 = \bar{k}_x^2 + \bar{k}_y^2$, $\tilde{\sigma}^2 = \tilde{\sigma}_x^2 + \tilde{\sigma}_y^2$, and $\tilde{\sigma}_{xy} = \tilde{\sigma}_x\tilde{\sigma}_y$. By solving Ω from (61) and substituting that into

the left-hand side of Eq. (60), after some algebraic calculations, we easily get

$$-\left[\beta^4\bar{k}_x^2\bar{k}_y^2\tilde{\sigma}^2+\beta^4\tilde{\sigma}_{xy}\left(\bar{k}_x^4+\bar{k}_y^4\right)+\beta^2\bar{k}^2\left(4\tilde{\sigma}_{xy}^2+2\tilde{\sigma}_{xy}\tilde{\sigma}^2\right)\right.$$
$$\left.+4\tilde{\sigma}_{xy}^2\tilde{\sigma}^2+\tilde{\sigma}_{xy}\left(\tilde{\sigma}^4+4\tilde{\sigma}_{xy}^2\right)\right]/(\tilde{\sigma}_x+\tilde{\sigma}_y)^2=0.$$

It is easy to see that the above is not possible for any positive nonzero $\tilde{\sigma}_x$, $\tilde{\sigma}_y$ and any real values of $\bar{k}_x$, $\bar{k}_y$. This means that (58) does not admit $\bar{\omega}$ with a positive imaginary part.

Now to study the stability of (35), we use a similar method employed in [18]. Define

$$F(\omega)\equiv(\omega+i\sigma_y)^2-\beta^2\frac{(\omega+i\sigma_y)^2}{(\omega+i\sigma_x)^2}\left(k_x+\frac{M}{1-M^2}\omega\right)^2 \tag{62}$$

and rewrite (35) as

$$F(\omega)=\beta k_y^2. \tag{63}$$

We show that $F(\omega)$ maps the upper-half ω-plane into a complex domain that excludes the real positive axis, as illustrated in Fig. 14, and therefore any solution of ω with a positive imaginary part is not possible for (63). Consider $F(\omega)$ and its counterpart in the transformed variables,

$$\bar{F}(\bar{\omega})=(\bar{\omega}+i\sigma_y)^2-\beta^2\frac{(\bar{\omega}+i\sigma_y)^2}{(\bar{\omega}+i\sigma_x)^2}\bar{k}_x^2.$$

Since (58) does not have any $\bar{\omega}$ with a positive imaginary part, $\bar{F}(\bar{\omega})$ will map the real $\bar{\omega}$-axis and above into a domain that excludes the real positive axis. Now, by the fact that the real ω-axis will be mapped similarly under $F(\omega)$ and $\bar{F}(\bar{\omega})$, it follows that $F(\omega)$ will, too, map the upper-half ω-plane to a domain that excludes the real positive axis. Hence, it is not possible for (63), and thus (35), to have ω with a real positive imaginary part.

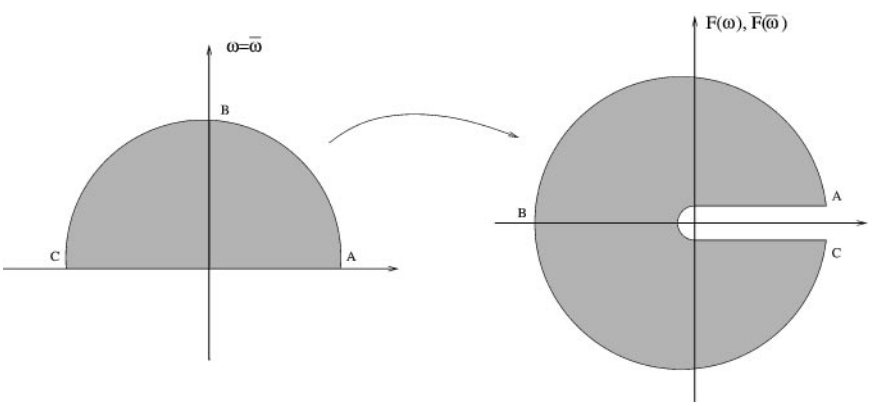

FIG. 14. Schematic drawing of mappings under $F(\omega)$ and $\bar{F}(\bar{\omega})$.

APPENDIX 2: MATRIX NORMS

For the L_2 norm of a diagonal matrix, we have

$$\|k_x \Lambda^{-1}\| = \left\| \begin{pmatrix} \frac{1}{M} & 0 & 0 & 0 \\ 0 & \frac{1}{M} & 0 & 0 \\ 0 & 0 & \frac{k_x}{Mk_x + k} & 0 \\ 0 & 0 & 0 & \frac{k_x}{Mk_x - k} \end{pmatrix} \right\| \leq C_0, \tag{64}$$

where $C_0 = \max(\frac{1}{M}, \frac{1}{1-M})$. Further, by

$$\left| \frac{1 - e^{-i\alpha t}}{\alpha} \right| = \left| \frac{2ie^{-i\alpha t/2} \sin\left(\frac{\alpha t}{2}\right)}{\alpha} \right| < t,$$

where α is a real number, we have

$$\|(\mathbf{I} - e^{-i\Lambda t})\Lambda^{-1}\| = \left\| \begin{pmatrix} \frac{1 - e^{-iMk_x t}}{Mk_x} & 0 & 0 & 0 \\ 0 & \frac{1 - e^{-iMk_x t}}{Mk_x} & 0 & 0 \\ 0 & 0 & \frac{1 - e^{-i(Mk_x + k)t}}{Mk_x + k} & 0 \\ 0 & 0 & 0 & \frac{1 - e^{-i(Mk_x - k)t}}{Mk_x - k} \end{pmatrix} \right\| < t. \tag{65}$$

ACKNOWLEDGMENT

This work was supported in part by NASA Grant NAG-1-01044.

REFERENCES

1. K. W. Thompson, Time-dependent boundary conditions for hyperbolic systems II, *J. Comput. Phys.* **89**, 439 (1990).
2. M. B. Giles, Non-reflecting boundary conditions for Euler equation calculations, *AIAA J.* **28**, 2050 (1990).
3. T. J. Poinsot and S. K. Lele, Boundary conditions for direct simulations of compressible viscous flows, *J. Comput. Phys.* **101**, 104 (1992).
4. R. L. Higdon, Numerical absorbing boundary conditions for the wave equation, *Math Comput.* **49**, 65 (1987).
5. A. Bayliss and Eli Turkel, Radiation boundary conditions for wave-like equations, *Comm. Pure Appl. Math.* **33**, 708 (1980).
6. B. Enquist and A. Majda, Absorbing boundary conditions for the numerical simulation of waves, *Math. Comput.* **31**, 629 (1977).
7. T. Hagstrom and S. I. Hariharan, Accurate boundary conditions for exterior problems in gas dynamics, *Math. Comput.* **51**, 581 (1988).
8. C. K. W. Tam and J. C. Webb, Dispersion-relation-preserving schemes for Computational acoustics, *J. Comput. Phys.* **107**, 262 (1993).
9. M. Israeli and S. Orszag, Approximation of radiation boundary conditions, *J. Comput. Phys.* **41**, 115 (1981).
10. T. Colonious, S. K. Lele, and P. Moin, Boundary conditions for direct Computation of aerodynamic sound generation, *AIAA J.* **31**, 1574 (1993).

11. C. L. Streett and M. G. Macaraeg, Spectral multi-domain for large-scale fluid dynamics simulations, *Int. J. Appl. Numer. Math.* **6**, 123 (1989).
12. S. Ta'asan and D. M. Nark, *An Absorbing Buffer Zone Technique for Acoustic Wave Propagation*, AIAA Paper 95-0164, 1995.
13. J.-P. Berenger, A perfectly matched layer for the absorption of electromagnetic waves, *J. Comput. Phys.* **114**, 185 (1994).
14. F. Q. Hu, On absorbing boundary conditions of linearized Euler equations by a perfectly matched layer, *J. Comput. Phys.* **129**, 201 (1996).
15. F. Q. Hu, *On perfectly matched layer as an Absorbing Boundary Condition*, AIAA Paper 96-1664, 1996.
16. S. Abarbanel, D. Gottlieb, and J. S. Hesthaven, Well-posed perfectly matched layers for advective acoustics, *J. Comput. Phys.* **154**, 266 (1999).
17. E. Turkel and A. Yefet, Absorbing PML boundary layers for wave-like equations, *Appl. Numer. Math.* **27,** 533 (1998).
18. C. K. W. Tam, L. Auriault, and F. Cambulli, Perfectly Matched Layer as an absorbing boundary condition for the linearized Euler equations in open and ducted domains, *J. Comput. Phys.* **144**, 213 (1998).
19. S. Abarbanel and D. Gottlieb, A mathematical analysis of the PML method, *J. Comput. Phys.* **134**, 357 (1997).
20. J. S. Hesthaven, On the analysis and construction of perfectly matched layers for the linearized Euler equations, *J. Comput. Phys.* **142**, 129 (1998).
21. F. Collino and P. Monk, The perfectly matched layer in curvilinear coordinates, *SIAM J. Sci. Comput.* **19**(6), 2016 (1998).
22. S. D. Gedney, An anisotropic perfectly matched layer-absorbing medium for the truncation of FDTD lattices, *IEEE Trans. Antennas Propagation* **44**, 1630 (1996).
23. L. Zhao and A. C. Cangellaris, GT-PML: generalized theory of perfectly match layers and its application to the reflectionless truncation of finite-difference time-domain grids, *IEEE Trans. Microwave Theory Tech*. **44**, 2555 (1996).
24. R. W. Ziolkowski, Time-derivative Lorentz material model-based absorbing boundary condition, *IEEE Trans. Antennas Propagation* **45**, 1530 (1997).
25. P. M. Morse and K. U. Ingard, *Theoretical Acoustics* (McGraw-Hill, New York, 1968).
26. J. Lighthill, *Waves in Fluids* (Cambridge University Press, Cambridge, 1978).
27. G. B. Whitham, *Linear and Nonlinear Waves* (Wiley, New York, 1974).
28. S. I. Hariharan, J. R. Scott, and K. L. Kreider, A potential-theoretic method for far-field sound radiation calculations, *J. Comput. Phys.* **164**, 143 (2000).
29. J. C. Strikwerda, *Finite Difference Schemes and Partial Differential Equations* (Wadsworth Belment, CA, 1989).
30. B. Gustafsson, H. O. Kreiss, and J. Oliger, *Time Dependent Problems and Difference Methods* (Wiley, New York, 1995).
31. J. Gary, On boundary conditions for hyperbolic difference schemes, *J. Comput. Phys.* **26**, 339 (1978).
32. F. Q. Hu, M. Y. Hussaini, and J. L. Manthey, Low-dissipation and low dispersion Runge–Kutta schemes for Computational acoustics, *J. Comput. Phys.* **124**, 177 (1996).
33. F. Q. Hu and J. L. Manthey, Application of PML absorbing boundary conditions to the Benchmark problems of Computational Aeroacoustics, in *Second Computational Aeroacoustics (CAA) Workshop on Benchmark Problems, 1997*, edited by C. K. W. Tam and Hardin (NASA CP 3352) pp. 119–151.